INTERNATIONAL JOURNAL FOR NUMERICAL METHODS IN FLUIDS, VOL. 20, 573–595 (1995)

THERMO-HYGRO-MECHANICAL ANALYSIS OF CONCRETE

PAOLO BAGGIO

Ist. di Fisica Tecnica, Facoltà di Ingegneria, Università di Padova, Via Venezia 1, 35131 Padova, Italy

CARMELO E. MAJORANA AND BERNHARD A. SCHREFLER

Ist. di Scienza e Tecnica delle Costruzioni, Facoltà di Ingegneria, Università di Padova, Via F. Marzolo 9, 35131 Padova, Italy

SUMMARY

The computational analysis of thermohygrometric and mechanical behaviour of concrete structures is carried out by means of the finite element method. To evaluate the thermal and hygral performance of this material together with the damage and creep effects, the knowledge of the heat and moisture transfer processes taking place inside the medium is first required and then the consequent mechanical behaviour can be analysed. The theoretical approach used to obtain the governing differential equations for heat and moisture transfer is based on the procedure of averaging continuum equations applied to heat and mass transfer and drying processes. According to that model the same set of equations is used to represent both the saturated zone (if present), the unsaturated one and the water-vapour phase changes. The mechanical formulation is based on the virtual work principle and incorporates Prony–Dirichlet series expansion to represent the relaxation or creep functions, avoiding the memorization of the whole strain or stress history. Damage effects are taken into account within a coupled formulation, following a procedure presented in a previous paper. At this preliminary stage the analysis is performed in two stages (first the heat and mass transfer and then the mechanical analysis) using two FEM computer codes in sequence to apply the proposed approach to structures of any shape.

KEY WORDS: concrete; porous media; heat and moisture transfer; damage; creep

INTRODUCTION

Moisture in concrete structures arises from the combined action of different causes such as the initial moisture content (due to the manufacturing process), rainwater infiltration, surface condensation (when the surface temperature approaches the dew point of the surrounding air), capillary rising and capillary condensation (due to meniscus curvature inside pores induced by surface tension that alter the equilibrium between the liquid water and the partial pressure of the water vapour). The effect of moisture on building structures is to lower thermal resistance (increasing heat losses) and to induce damages (such as blister formation, dimensional change, degradation of strength and mold growth). Moreover creep and shrinkage of concrete are strongly related to moisture transfer phenomena. To evaluate the thermal and moisture transmission behaviour and the related stresses and strains of porous building materials and to comprehend and/or anticipate the moisture induced degradation a thorough understanding of the heat and moisture transfer phenomena taking place inside them is required. Therefore theoretical

CCC 0271–2091/95/060573–23

Received 4 August 1994
Revised 2 November 1994

models allowing to analyse and forecast the combined heat and mass transfer in porous media are needed.

Such phenomena are quite complex because they involve not only heat conduction and vapour diffusion (as proposed by Glaser[1-3]) but, as suggested by Philip and De Vries[4] and De Vries,[5] also heat convection, liquid water flow because of pressure gradients or capillary effects and latent heat transfer due to water phase change (evaporation and condensation) inside the pores. It is now assumed that moisture transfer in porous media cannot be interpreted with a purely diffusive model (see the thorough review presented by Whitaker[6] and the numerous references cited in his paper) and that a formulation based on diffusion like equations, as the one presented by Luikov,[7] implies the use of transport coefficients that lump together different transport mechanisms, masking the dependence on the different controlling variables, as observed by Chen and Pei.[8] As Whitaker[6] pointed out, good agreement between the theory and experiments can be obtained with such models only by allowing each transport coefficient ('diffusivity') to be a complex and highly non-linear function of the moisture content and temperature. This results also from the theory proposed by Philips and De Vries[4] and De Vries.[5]

The theoretical model used here is the one proposed by Whitaker[6,9] which was developed starting from the equations of continuum mechanics, following the approach originally proposed to study the dynamics of water flow in unsaturated soils by Bear,[10,11] Bear and Bachmat[12-14] and Hassanizadeh and Gray.[15-17] Such approach has been applied by Whitaker[6,9] and, more recently, by other authors (Chen and Pei,[8] Nasrallah and Perre,[18] Ilic and Turner[19,20]) to drying problems.

The mechanical analysis is carried out to calculate stresses and strains due to the variations of moisture and temperature inside the material. As far as the constitutive relationship is concerned, an analytical formulation is adopted here to take into account viscoelasticity and damage. The formulation is based on the approximate evaluation of the superposition integral. In Majorana[21] viscoelastic models including isotropic damage effects were considered, by introducing in the stress–strain relationship expressed as Stiltjes integrals the effective stress concept of Lemaitre,[22] or forms of the relaxation or creep functions which include already damage, as in Bazant and Prasannan.[23] Note that the above meaning of effective stress differs from the usual one in soil mechanics. In this paper anisotropic damage is taken into account, following Ramtani[24] and is further coupled with viscosity[25] to better model the time transient behaviour of concrete. The full two-step model allows to simulate by means of the finite element method the evolution of temperature, moisture content, the global kinetic of the process and stresses and strains. The finite element technique was previously successfully applied to porous media thermomechanical problems in References 26 and 27.

HEAT AND MASS TRANSFER FORMULATION

The formulation of heat and mass transfer in porous media is obtained starting from the appropriate equations in local form expressing the laws of continuum physics (see, for example Reference 28), specifically the continuity equation for each considered species, the Navier–Stokes equation for quasi-steady creeping flow (i.e. with the time dependent and convective terms neglected) and the energy equation (enthalpy balance) with reversible work, viscous dissipation, and other irreversible sources neglected. In general such equations cannot be solved because of the complex geometry of the porous media, but using the volume averaging technique[15-17,6] we can obtain equations averaged on a *representative elementary volume* (REV)[15] of the porous medium.

Following Whitaker[6] and using the multiphase Darcy's law applied to the liquid phase:

$$\mathbf{v}_l = -\frac{KK_{rl}}{\mu_l}(\nabla P_g - \nabla P_c - \rho_l \mathbf{g})$$

and applied to the gas phase:

$$\mathbf{v}_g = -\frac{KK_{rg}}{\mu_g}(\nabla P_g - \rho_g \mathbf{g})$$

where $\mathbf{v}_l$ and $\mathbf{v}_g$ are the velocities, respectively, of the liquid and the gas phase, the capillary pressure equation is $P_c = P_g - P_l$, where P_l the pressure of the liquid-phase (water), and finally, the equation of state of perfect gas, applied to dry air $P_{ga} = \rho_{ga} TR/M_a$, to vapour $P_{gw} = \rho_{gw} TR/M_w$ and moist air $P_g = P_{ga} + P_{gw}$, $\rho_g = \rho_{ga} + \rho_{gw}$ the conservation equations can be written as follows (see References 6, 9 and 18–20 for their derivation):

dry air conservation

$$\phi \frac{\partial}{\partial t}[\rho_{ga}(1-S)] - \nabla \cdot \left(\rho_{ga} \frac{KK_{rg}}{\mu_g} \nabla(P_g)\right) + \nabla \cdot \left(\rho_g \frac{M_a M_v}{M^2} D_{eff} \nabla\left(\frac{P_{gw}}{P_g}\right)\right) = 0 \tag{1}$$

water (liquid-vapour) species conservation

$$\phi \frac{\partial}{\partial t}[\rho_{gw}(1-S)] - \nabla \cdot \left(\rho_{gw} \frac{KK_{rg}}{\mu_g} \nabla(P_g)\right) - \nabla \cdot \left(\rho_g \frac{M_a M_v}{M^2} D_{eff} \nabla\left(\frac{P_{gw}}{P_g}\right)\right)$$
$$= -\phi \rho_l \frac{\partial S}{\partial t} + \nabla \cdot \left(\rho_l \frac{KK_{rl}}{\mu_l}(\nabla(P_g) - \nabla(P_c) - \mathbf{g})\right) \tag{2}$$

energy conservation (enthalpy balance)

$$\rho C_p \frac{\partial T}{\partial t} - \left[C_{pw}\rho_w \frac{KK_{rl}}{\mu_l}(\nabla(P_g) - \nabla(P_c) - \mathbf{g}) + C_{pg}\rho_{gw} \frac{KK_{rg}}{\mu_g} \nabla(P_g)\right] \cdot \nabla(T)$$
$$- \nabla \cdot (\lambda_{eff} \nabla(T)) = \Delta h_{vap}\left[\phi \rho_l \frac{\partial S}{\partial t} + \nabla \cdot \left(\rho_l \frac{KK_{rl}}{\mu_l}(\nabla(P_g) - \nabla(P_c) - \mathbf{g})\right)\right] \tag{3}$$

These equations must be supplemented with thermodynamic relationships (perfect gases' law and Clausius Clapeyron equation) and constitutive equations (that express the relationships between relative permeabilities K_{rg}, K_{rl}, saturation S, partial vapour pressure P_{gw}, and capillary pressure P_c), needed for the closure of the model. For details see the References 6, 9, 10, 18 and 19 and Baggio and Bonacina.[29] This model employs the same equations, (1)–(3), to represent both the unsaturated and the saturated zones (if present). Phase-change phenomena are also taken in account.

For the relationship between the relative humidity and the capillary pressure in the concrete pores the Kelvin–Laplace law is assumed to be valid:

$$R.H. = \frac{P_{gw}}{P_{gws}} = \exp\left(-\frac{P_c M_w}{\rho_l RT}\right) \tag{4}$$

Since the capillary pressure P_c is equal to the *water potential* Ψ multiplied by a constant (i.e. $P_c = -\rho_l \Psi$), equation (4) can be used also below the capillary region (see Appendix I).

MECHANICAL FORMULATION

The set of equations governing thermohygrometric and mechanical behaviour of concrete in viscoelastic range without damage effects has been presented in References 30 and 31 where a different thermohygrometric model was used. In Reference 21, damage influences on the constitutive relationship and on some thermohygrometric and mechanical characteristics such as diffusivities and thermal/hygral expansion coefficients have been taken into account, considering the isotropic damage model of Mazars and Pijaudier–Cabot.[32] Here a formulation based on the finite element technique is used taking into account geometrical non-linearities, as well as viscoelasticity coupled with damage. The geometrically non-linear approach is useful because in anisotropic models the principal directions of damage rotate. Hence the variables which control the evolution of damage (true strains), rotate also and must be referred to evolving geometrical configurations even if strains remain small. Here we consider such situations with small strains, hence the heat and mass transfer formulation stated in previous section, within a linearized geometrical framework, is considered sufficiently accurate.

In the adopted geometrically non-linear description of the problem, the Cauchy stress tensor $\boldsymbol{\sigma}$ is replaced by the second Piola–Kirchhoff stress tensor $\mathbf{S}$ with the associated Lagrange strains E, both referred to the material configuration.[33] The stress and strain tensors $\mathbf{S}$ and $\mathbf{E}$ are energetically conjugate and may define covariant constitutive relationships, preserving material frame indifference under any diffeomorphism.[34] The geometry is referred to a cartesian orthogonal frame, as a particular case of the more general riemannian one.

The total lagrangian formulation has been used to calculate the desired quantities with reference to the initial undeformed configuration. The approximate equation of motion can be written hence as follows:

$$\int_V \mathbf{S}^0 \delta E^0 \, \mathrm{d}V_0 = \mathbf{R} \tag{5}$$

where $\mathbf{R}$ is the external virtual work evaluated at time $t + \Delta t$. The strain variation and stress components are

$$\delta E^0_{ij} = \tfrac{1}{2}\delta \left[u^0_{i,j} + u^0_{i,j} + u^0_{k,i} u^0_{k,j}\right] \tag{6}$$

$$S^0_{ij} = |J^0| \, \bar{x}^0_{i,m} \sigma_{mn} \bar{x}^0_{j,n} \tag{7}$$

with u_{ij} displacement components and x_i spatial co-ordinates.

The viscoelastic constitutive relationship taking into account damage effects presented in References 21 and 31 is rewritten in terms of finite strain formulation, using the second (symmetric) Piola–Kirchhoff stress tensor $\mathbf{S}$ and the associated lagrangian strains.[35] The coupling of viscoelasticity and damage follows a procedure similar to that employed in Reference 36. In that paper, viscous response was characterized by a linear rate constitutive equation and a convolution representation to generalize viscoelastic models with linearized kinematics to the case of non-linear geometry. Continuum damage mechanics was further employed to take into account the degradation of the stiffness. In numerical perspective, a local additive decomposition of the stress tensor into initial and non-equilibrium parts was considered. This model allows to recover the elastic behaviour at the end of very slow and at the beginning of very fast processes. Elastic damage at finite strains is incorporated in the procedure, reducing the free energy by the factor $\|\mathbf{1}–\mathbf{D}\|$, with $\mathbf{D}$ is the damage tensor. As in the above paper, the damage model is based here on maximum strain concept. A computational simplification is introduced where damage tensor $\mathbf{D}$ is taken constant within a time step increment. With this hypothesis $\mathbf{D}$ is evaluated once

at each step without additional iterations at the end of each time increment. The following viscoelastic-damage coupled matrix is hence obtained:

$$\int_V \delta E^{0\mathrm{T}} \left\{ \{\mathbf{1} - \mathbf{D}^0\} \left[\mathbf{C}_1 \cdot {}^t E^0 + \mathbf{C}_2 \cdot E^{00} + \mathbf{C}_3 \cdot {}^t E^0 - \frac{1}{2} \sum_{\mu=1}^{N} \mathbf{Q}_\mu^0 + \frac{1}{2} \sum_{\mu=1}^{N} \mathbf{R}_\mu^0 \right] \right\} \mathrm{d}V_0 = \mathbf{R} \quad (8)$$

where $\mathbf{C}_1$, $\mathbf{C}_2$ and $\mathbf{C}_3$ do not depend on the deformations[21] (their expressions are reported in Appendix II); the terms $\mathbf{E}^{00}$ are imposed strains, hence in the previous equation they must be interpreted as known terms, like the term $\sum_{\mu=1}^{N} \mathbf{R}_\mu^0$ which is dependent on such strains ($\mu = 1, N$ Maxwell chain units); finally the terms ${}^t\mathbf{E}^0$ and $\sum_{\mu=1}^{N} \mathbf{Q}_\mu^0$ (where the last one depends on the calculated strains) are to be interpreted again as known terms. $\mathbf{D}^0$ is the damage tensor.

Using the incremental decompositions $E_{ij}^0 = {}^t E_{ij}^0 + \Delta E_{ij}^0$, $\Delta E_{ij}^0 = \Delta \varepsilon_{ij}^0 + \Delta \eta_{ij}^0$ (with ε_{ij}, η_{ij} linear and non-linear parts of the strain tensor, respectively), observing that for our purpose $\delta E_{ij}^0 \approx \delta \Delta E_{ij}^0$, and assuming further that $\delta \Delta E^{0\mathrm{T}} = \delta \Delta \varepsilon^{0\mathrm{T}}$, and $\{\mathbf{1} - \mathbf{D}^0\} \mathbf{C}_1^0 \cdot \Delta E^0 = \{\mathbf{1} - \mathbf{D}^0\} \mathbf{C}_1^0 \cdot \Delta \varepsilon^0$ the following equation of motion is obtained:

$$\begin{aligned} &\int_V \delta \Delta \varepsilon^{0\mathrm{T}} \{ \{\mathbf{1} - \mathbf{D}^0\} \mathbf{C}_1 \cdot \Delta \varepsilon^0 \} \, \mathrm{d}V_0 \\ &\quad + \int_V \delta \Delta \boldsymbol{\eta}^{0\mathrm{T}} \left\{ \{\mathbf{1} - \mathbf{D}^0\} \left[\mathbf{C}_1 \cdot {}^t E^0 + \mathbf{C}_2 E^{00} + \mathbf{C}_3 \cdot {}^t E^0 - \frac{1}{2} \sum_{\mu=1}^{N} \mathbf{Q}_\mu^0 + \frac{1}{2} \sum_{\mu=1}^{N} \mathbf{R}_\mu^0 \right] \right\} \mathrm{d}V_0 \\ &\quad = \mathbf{R} - \int_V \delta \Delta \varepsilon^{0\mathrm{T}} \left\{ \{\mathbf{1} - \mathbf{D}^0\} \left[\mathbf{C}_1 \cdot {}^t \mathbf{E}^0 + \mathbf{C}_2 \cdot E^{00} + \mathbf{C}_3 \cdot {}^t E^0 - \frac{1}{2} \sum_{\mu=1}^{N} \mathbf{Q}_\mu^0 + \frac{1}{2} \sum_{\mu=1}^{N} \mathbf{R}_\mu^0 \right] \right\} \mathrm{d}V_0 \end{aligned} \quad (9)$$

EQUATION DISCRETIZATION AND NUMERICAL SOLUTION

The numerical solution is carried out by the finite element technique in two uncoupled steps.

Heat and mass transfer solution

As far as the thermohygrometric problem is concerned, the variables P_g, P_c, and T are approximated with the expansions:

$$P_g \approx \sum N_i P_{gi} = \mathbf{N}\mathbf{P}_g, \quad P_c \approx \sum N_i P_{ci} = \mathbf{N}\mathbf{P}_c, \quad T \approx \sum N_i T_i = \mathbf{N}\mathbf{T} \quad (10)$$

where N are the shape functions,[34] P_{gi}, P_{ci}, T_i the nodal values of the variables and $\mathbf{P}_g$, P_c, T_i the vectors of the nodal values. The semi-discretization of the conservation equations (1)–(3) (and of the other ones required to complete the model) with the standard Galerkin method (weighted residuals)[37] results in a non-symmetric, non-linear coupled system of ordinary differential equations of the form:

$$\mathbf{C}(\mathbf{x}) \frac{\mathrm{d}\mathbf{x}}{\mathrm{d}t} + \mathbf{K}(\mathbf{x})\mathbf{x} + \mathbf{f}(\mathbf{x}) = 0 \quad (11)$$

where

$$\mathbf{x} = \begin{Bmatrix} \mathbf{P}_g \\ \mathbf{P}_c \\ \mathbf{T} \end{Bmatrix} \quad (12)$$

and the definitions of the non-linear (matrix) coefficients $\mathbf{C}(\mathbf{x})$, $\mathbf{K}(\mathbf{x})$ and $\mathbf{f}(\mathbf{x})$ are reported elsewhere.[29]

The time-discretization is accomplished through a fully implicit finite difference scheme, i.e. the terms in equation (11) are evaluated at the end of the interval $|t, t + \Delta t|$, where Δt is the time step.

Preliminary tests revealed that the Crank–Nicholson scheme (central differences) was unstable and was then abandoned. Considering the strong non-linearity of the system of equations (11) the solution is obtained with a Newton–Raphson method. Based on this discretization, the HMTRA research computer code has been developed for the solution of the non-linear and non-symmetrical system of equations governing heat and mass transfer.

The details pertaining equations, boundary conditions, discretization and computer code can be found in Reference 29.

Mechanical solution

As far as the mechanical problem is concerned the procedure used is described in what follows. By introducing discretization in space by means of finite elements, equation (9) becomes

$$\begin{aligned}&\left\{\int_V \left[\mathbf{B}_0 + \mathbf{B}_L\right]^T \{\mathbf{1} - \mathbf{D}^0\}\mathbf{C}_1 \left[\mathbf{B}_0 + \mathbf{B}_L\right] dV_0 \right.\\ &\left. + \int_V \mathbf{G}^T \left\{\{\mathbf{1} - \mathbf{D}^0\}\left[\mathbf{C}_1 \cdot {}^t\mathbf{E}^0 + \mathbf{C}_2 \cdot E^{00} + \mathbf{C}_3 \cdot {}^tE^0 - \frac{1}{2}\sum_{\mu=1}^{N} \mathbf{Q}_\mu^0 + \frac{1}{2}\sum_{\mu=1}^{N} \mathbf{R}_\mu^0\right]\right\} \mathbf{G}\, dV_0\right\} \Delta\mathbf{u}\\ &= \mathbf{R} - \int_V \left[\mathbf{B}_0 + \mathbf{B}_L\right]^T \left\{\{\mathbf{1} - \mathbf{D}^0\}\left[\mathbf{C}_1 \cdot {}^tE^0 + \mathbf{C}_2 \cdot E^{00} + \mathbf{C}_3 \cdot {}^tE^0 - \frac{1}{2}\sum_{\mu=1}^{N} \mathbf{Q}_\mu^0 + \frac{1}{2}\sum_{\mu=1}^{N} \mathbf{R}_\mu^0\right]\right\} dV_0\end{aligned} \tag{13}$$

In equation (13), $\mathbf{B}_0$, $\mathbf{B}_L$, $\mathbf{G}$ are the initial, linear and non-linear strain matrices, respectively. A complete description of the introduced relationships can be seen in Reference 35.

After solving the system of algebraic equations (13), the strains at time $t_{n+1} = t_n + \Delta t_n$ can be calculated as

$$\mathbf{E}(t_{n+1}) = [\mathbf{B}_0 + \mathbf{B}_L]\,\mathbf{u}(t_{n+1}) \tag{14}$$

The stresses are then obtained by the standard procedure for viscoelasticity with damage.[21,36,38] The procedures were implemented in the finite element code DAMVIS.

NUMERICAL COMPUTATIONS

Some numerical simulations were carried out starting from the data reported in Acker *et al.*[39] for a concrete cylinder where creep and shrinkage phenomena develop.

Considering the cylindrical shape of the sample, a mesh extended to a quarter of the cylinder of 72 (9×8) axisymmetric eight noded serendipity elements was used (Figure 1).

The sample was assumed to be initially at 99 per cent relative humidity and at a temperature of 22°C. The surrounding air was assumed to have the same temperature and a relative humidity equal to 50 per cent. A convective boundary condition for the temperature was imposed at the interface between the sample and the air with a surface heat exchange coefficient equal to $4\,\mathrm{W\,m^{-1}\,K^{-1}}$. The surface mass exchange coefficient for the water vapour was set equal to $0{\cdot}0036\,\mathrm{m\,s^{-1}}$. Heat generation and curing were not considered in the numerical examples, although the relative effects can be taken into account by the used program (see e.g. Reference 30).

The concrete was assumed to have a total porosity φ of 16·7 per cent, an absolute permeability K equal to $3{\cdot}97 \times 10^{-20}\,(\mathrm{m^2})$ and a dry thermal conductivity λ equal to $2{\cdot}5\,\mathrm{W\,m^{-1}\,K^{-1}}$. The

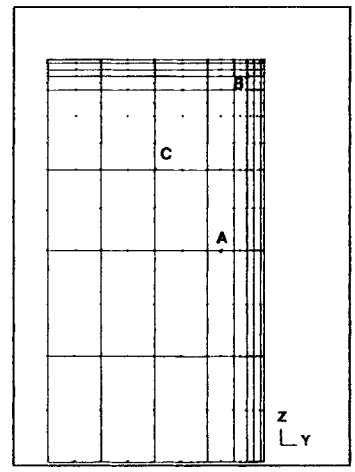

Figure 1. Finite element mesh of a quarter cylinder (axysimmetric)

diffusion of water vapour was assumed to take place in the part of the pores not filled with liquid and a tortuosity factor $\tau = 0{\cdot}25$ was considered to take in account the microstructure of concrete. The effective diffusivity was then set equal to $D_{\text{eff}} = \tau(1 - S)D_0$ where D_0 is the diffusivity of water vapour in air.

As far as damage is concerned different formulations were used (i.e. those due to Mazars,[32] and due to Kachanov and Kachanov–Rabotnov[25]) to take into account also time transient damage as occurs in primary, secondary and tertiary creep ranges.[40] The above models were chosen as examples because of their easy calibration for a given concrete. We emphasize again that the implemented procedure is general, hence in principle any type of damage relationship, depending on a given tensor (intended as a parameter) and time can be used. Non-local formulation of strain controlling damage was also incorporated (see Appendix III).

Tensile and compressive damage effects were considered and the following data were assumed: damage threshold $K = 0{\cdot}00011$, and $A_t = 0{\cdot}8$, $A_c = 1{\cdot}4$, $B_t = 2000$, $B_c = 1850$ (Mazar's model), $Ak_t = 0{\cdot}00011$, $Ak_c = 0{\cdot}0003$, $k = 9$, $r = 30$ (Kachanov and Rabotnov model), corresponding to compressive cylindrical strength of 35 MPa and a tensile strength of 3·5 MPa, characteristic length for non-local model $l = 2{\cdot}8$ cm. Several simulations have been carried out. Here two of them are reported as example. In Figures 2(a) and 2(b) the relative humidity profiles in the sample at different times (days) are presented.

The time transient relative humidity of a nodal point is shown in Figure 3 where a comparison between the purely diffusive model and the novel one (coupled heat and mass transfer including phase changes) is also demonstrated. The two approaches qualitatively agree quite well, although a direct comparison is not possible, since they are conceptually different. It should also be remarked that purely diffusive models only have been traditionally used for the analysis of mass transfer inside concrete.[41]

As far as the mechanical problem is concerned, the total damage of the outer zone of the cylinder can be seen in Figure 4 where damage versus radius of a transverse section of the cylinder is reported for different time values. The axial, hoop and radial stresses are shown in Figures 5–7. The results agree well with those found in Reference 39, both in terms of humidities and stresses. The non-local formulation assures that mesh-independent results can be obtained[21] (the influence

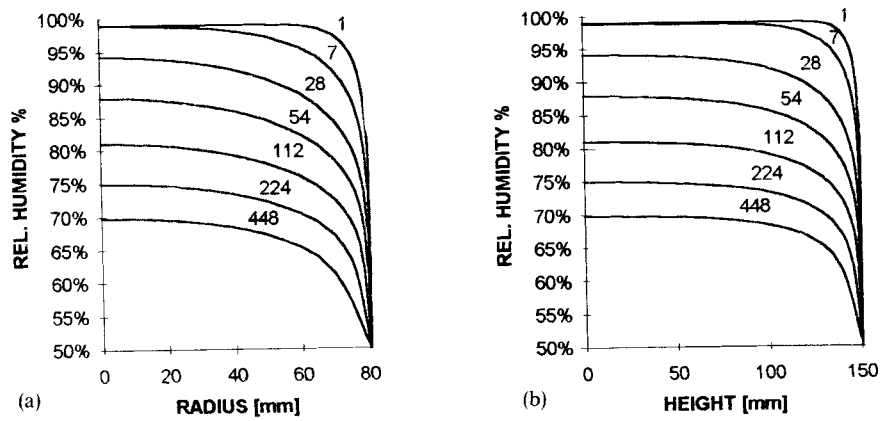

Figure 2. (a) Relative humidities versus radius; (b) Relative humidities versus height (time in days)

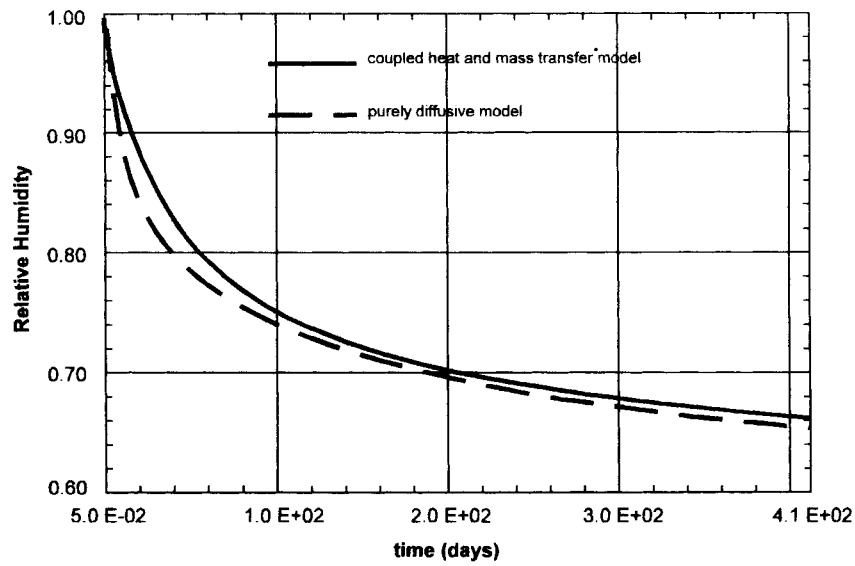

Figure 3. Time transient of relative humidity at nodal point A

radius considered is $r = 1{\cdot}5$ cm with 15 Gauss points involved instead of 80 if the whole domain is considered). Time transients of the vertical stress component at two nodal points are shown in Figures 8 and 9 comparing the purely diffusive model with the novel one.

The next example deals with massive concrete. The purely diffusive and the new model are used for comparison.

A concrete sample was assumed to be initially at a relative humidity of 99 per cent and at a temperature of 27°C. The surrounding air was assumed to have the same temperature and a relative humidity equal to 60 per cent.

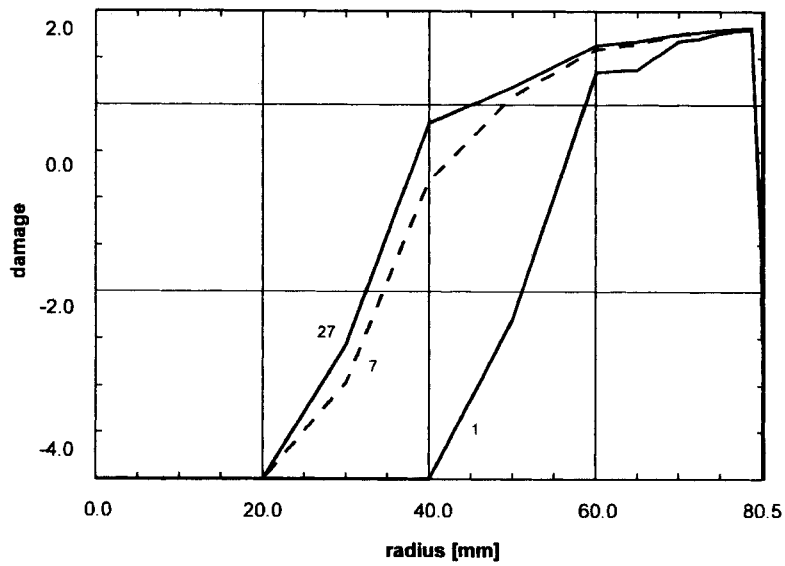

Figure 4. Damage versus radius at different times (days)

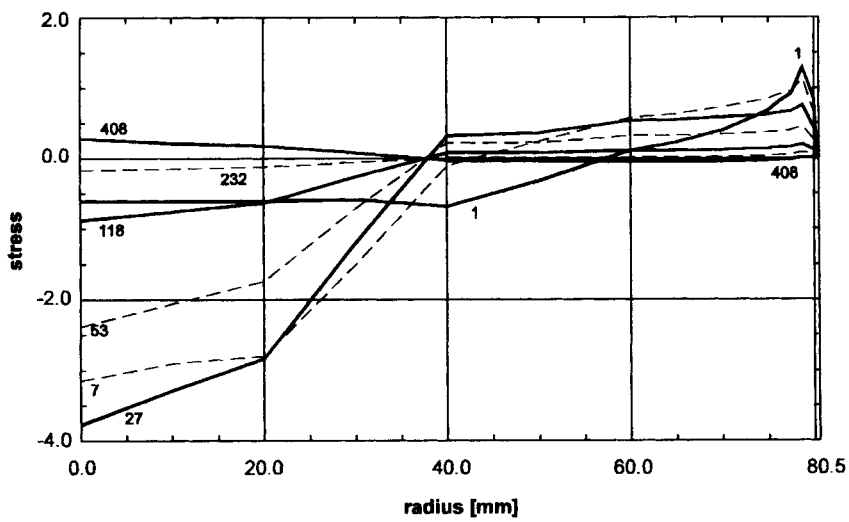

Figure 5. Axial stress versus radius at different times (days)

For comparison, in the purely diffusive model, the following properties were selected (corresponding to a concrete of better quality than the previous one, with compressive cylindrical strength equal to 55 MPa):

(1) Diffusivity at 28 days in saturated conditions depends on the concrete composition. In the actual case, a value of the diffusivity guaranteeing the maximum penetration of the hygrometric field inside the casting has been chosen as 20 mm^2/days.

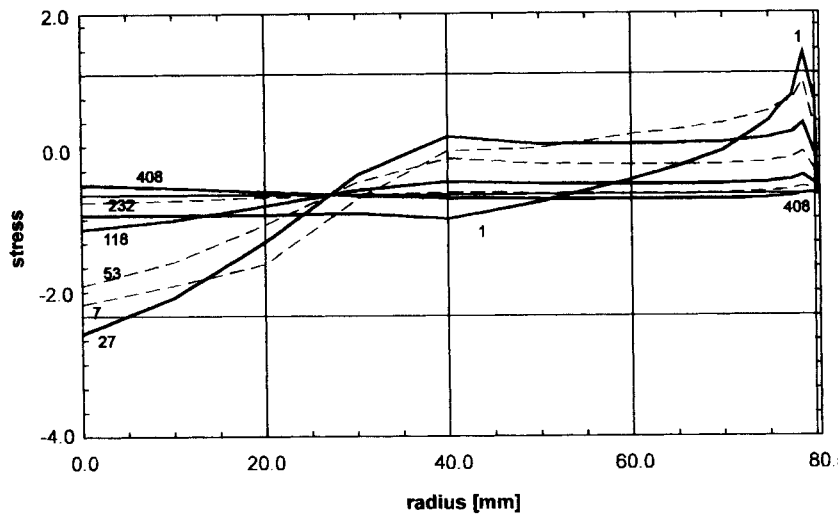

Figure 6. Hoop stress versus radius at different times (days)

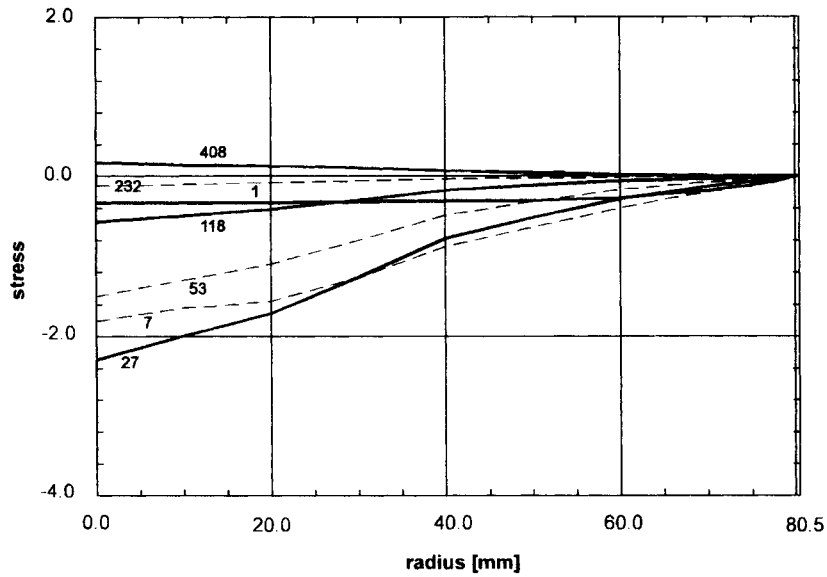

Figure 7. Radial stress versus radius at different times (days)

(2) Also the other parameters in the well known non-linear diffusion law,[21,42] i.e. α_0, h_c and n depend on the mix design. In particular, h_c is chosen as the mean value of the ambient and initial humidities, with $h_c = 0{\cdot}75$ for an environmental relative humidity equal to 0·5. The parameter n is usually recommended in the range 6–16; $n = 6$ has been taken here. Finally $\alpha_0 = 0{\cdot}005$.

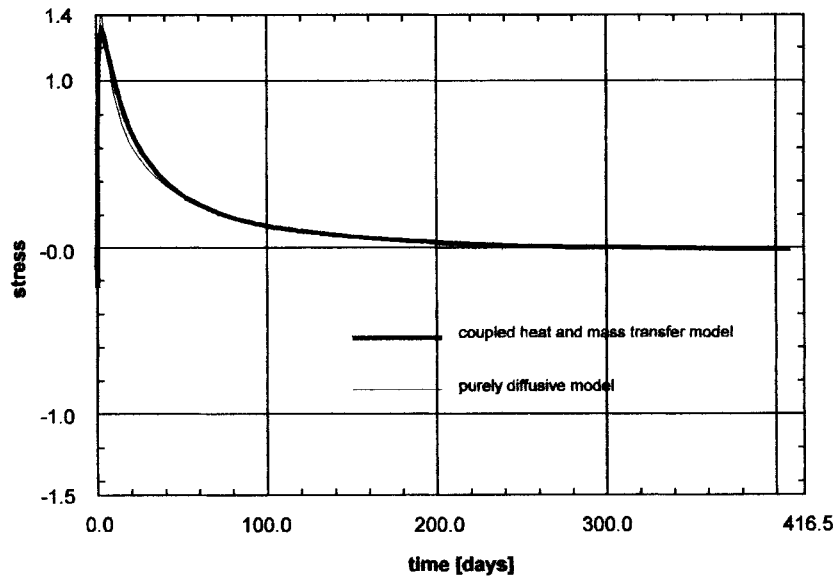

Figure 8. Time transient of axial stress at the top surface (nodal point B)

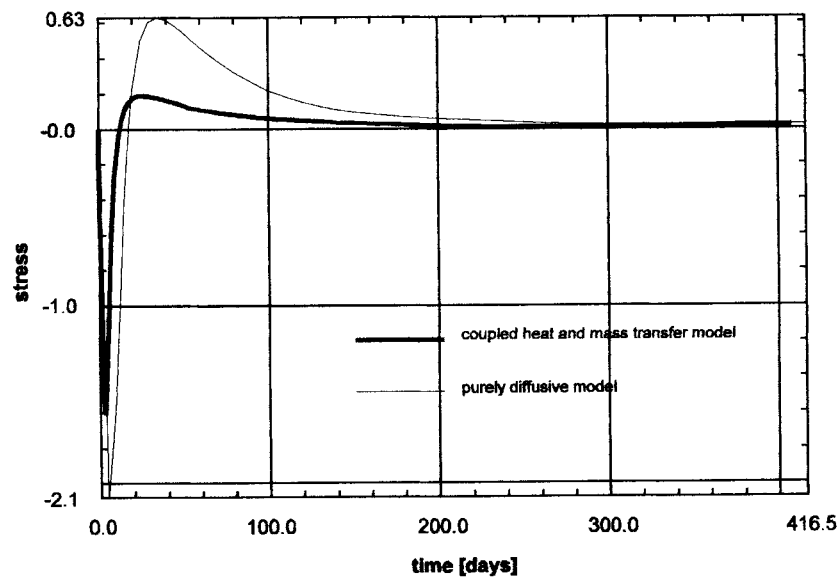

Figure 9. Time transient of axial stress at the top surface (nodal point C)

(3) Particularly important is the choice of the free shrinkage. This parameter can be considered as a constitutive property of the material; it is the shrinkage at $t = t_0$ in absence of inner stresses. Lower and upper limits of this parameter can be found in literature. Wittmann[43] shows a diagram of unrestrained shrinkage as a function of the relative humidity for

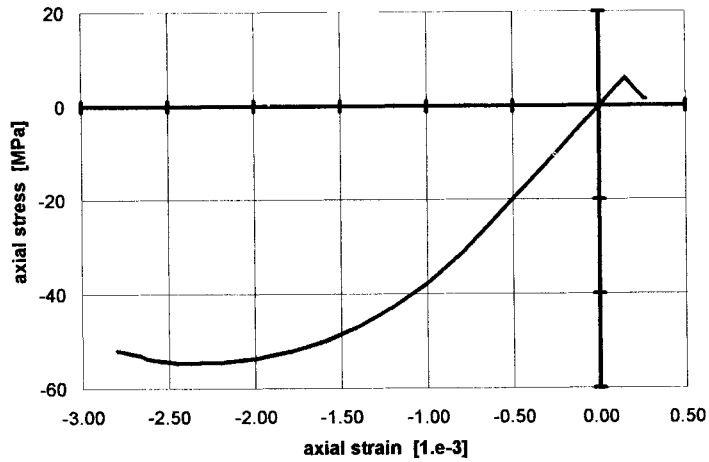

Figure 10. Assumed stress–strain relationship of concrete

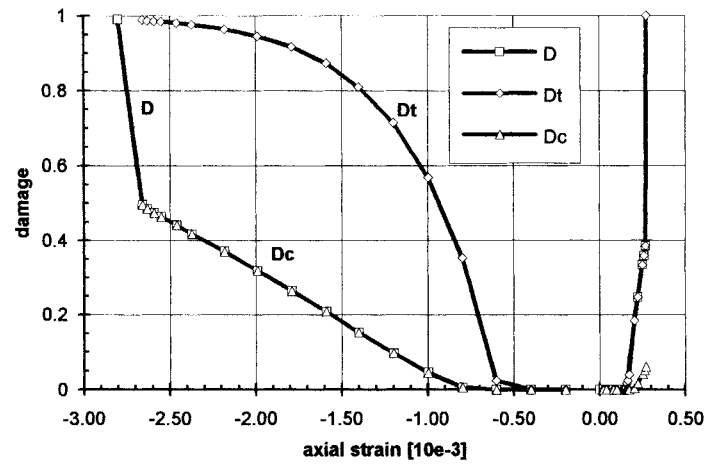

Figure 11. Damage versus strain in tension and compression (D_t = damage in tension, D_c = damage in compression, D = total damage)

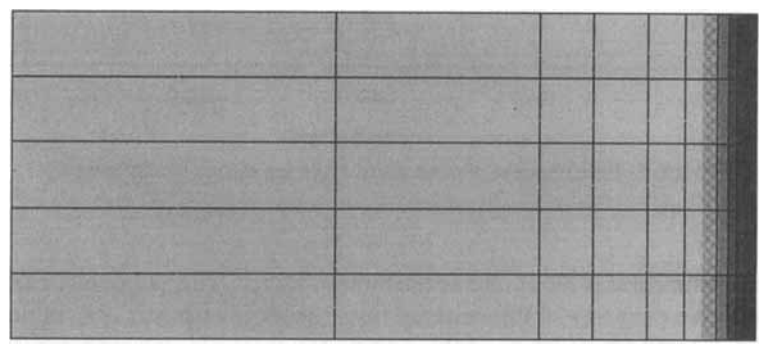

Figure 12. Finite element mesh in the intermediate zone of massive casting

a concrete with $w/c = 0{\cdot}35$, similar to that of the concrete used here. From the diagram it appears that the unrestrained shrinkage tends with a zero value of the relative humidity to 0·00035–0·004. Here a value of 0·002 has been taken, also based on existing relationships between shrinkage and water content variation.

Some preliminary analyses on cylindrical samples of limited dimensions (as those of the previous example) have been carried out for calibrating the stress–strain behaviour of the chosen concrete. In this case the sample is subjected to physical loads only, in order to keep out the effects

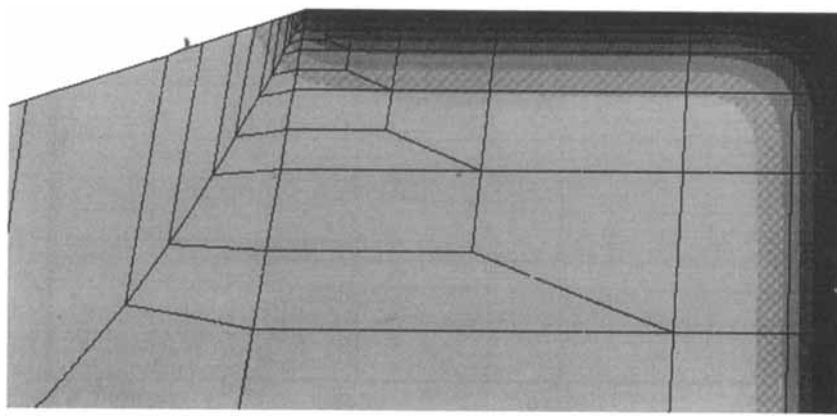

Figure 13. Finite element mesh in a corner zone of massive casting

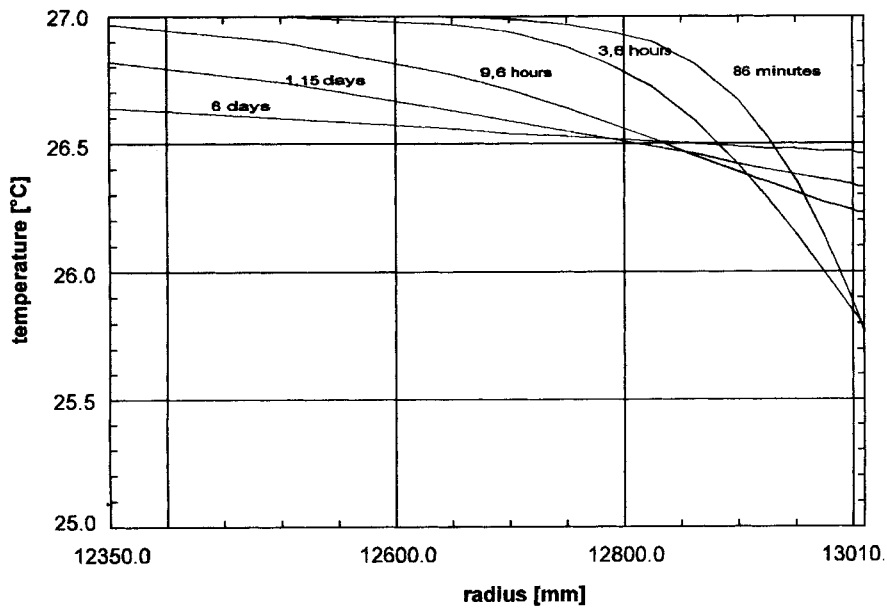

Figure 14. Temperatures versus radius at different times

of shrinkage and thermal variations. The applied load assumes different values, so as to induce various degrees of damage in the sample. It is hence possible to find the stress–strain relationship of Figure 10 together with the patterns of the compressive, tensile and total damages as function of the reference strain (Figure 11). The analysis of a concrete cylinder of large dimensions (massive concrete casting) has then been carried out taking the constitutive relationship of Figure 10 and

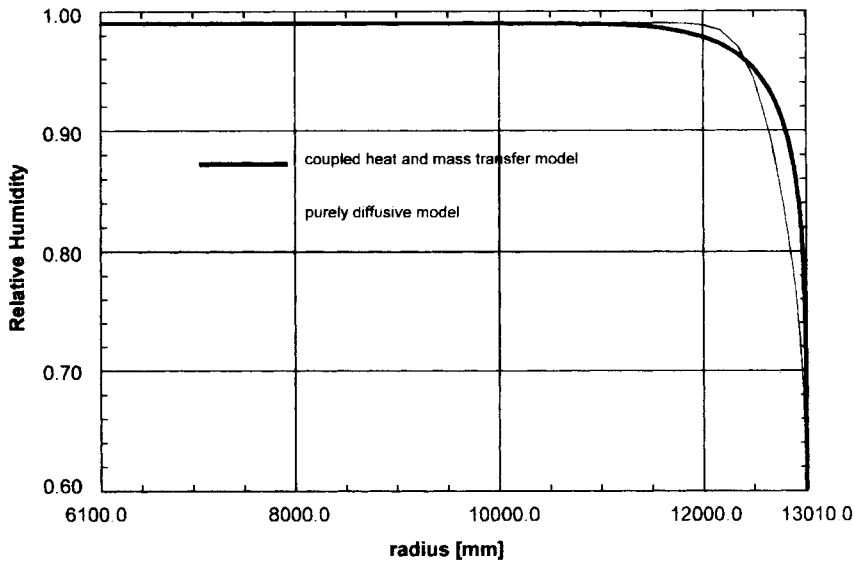

Figure 15. Relative humidities versus radius at 19 years

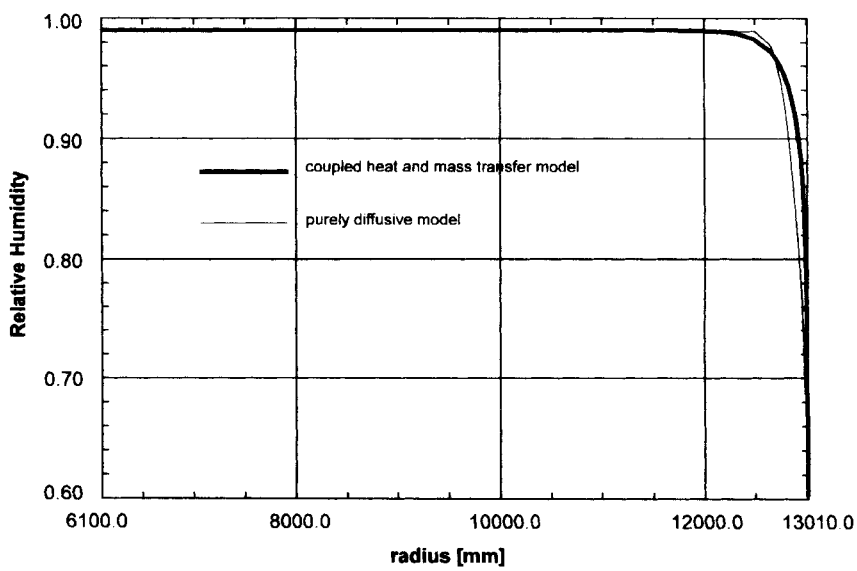

Figure 16. Relative humidities versus radius at 3·6 years

designing an appropriate mesh. Of this mesh, a strip representative of an intermediate zone where the fluxes are essentially one-dimensional is reported in Figure 12 and in Figure 13 a typical angular zone. The chosen finite elements are quadratic and integrated with a gaussian scheme with nine points for temperature and humidity and four points for displacements.

Time transients of the humidities, temperatures, displacements, stresses and strains are obtained, together with those of the damage of the employed material (Figures 14–18). The hygral exchange between the sample and the ambient appears in the outer zone of the cylinder only during the first 50 years after casting, letting the inner massive zone of the concrete in conditions of almost total saturation (99 per cent R.H.) as at the beginning of the process. The strip where the process is active is about 0·5 m for the thermohygral phenomenon and 1 m for the mechanical one. This is an accordance with the experimental findings of Mamillan and Boineau[41] and those of Acker.[39] The results also confirm the impossibility to proceed in the case of massive castings with calculations where mean values are taken along the thickness for phenomena of this kind.

The stress and strain states are found using the viscoelastic-damage model presented above. The evolution of the stress components show that the strength limit at tension can be reached. In such cases the onset of damage is predicted in the same regions. The strain components rapidly change from negative (due to compression) to positive (due to tension), together with local material damaging. Observing the stresses along a transverse section of the model, a stress penetration of about 1 m can be observed (see Figure 17). Compression, tension and total damage are compatible with the developed strains both in time and along significant sections. The damage starts at the time of occurrence of maximum strain at the boundary, which is about 10 days after casting. If wanted, maximum damage could be adequately controlled using better quality concretes.

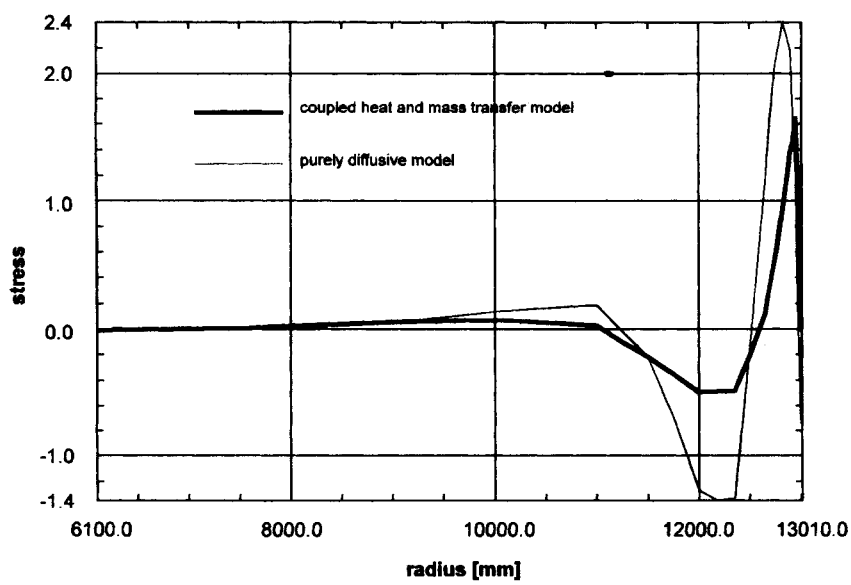

Figure 17. Radial profile of axial stress (MPa) at 18 years

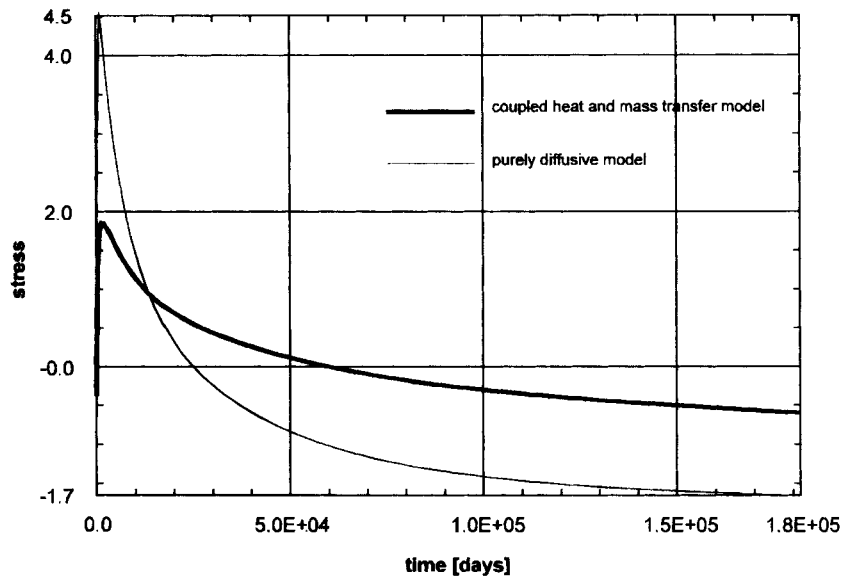

Figure 18. Axial stress versus 0·2 m below the middle point of the upper flat surface

CONCLUSIONS

An enhanced model which takes into account phase changes has been used here to simulate heat and mass transfer in porous materials and particularly in concrete. Compared to the traditional diffusive-only model such a procedure results in an improvement of the description of physical phenomena occurring in drying concrete, especially when temperature effects are important. It has to be pointed out that, even starting from isothermal initial conditions, heat transfer phenomena can take place because of phase changes (evaporation and condensation).

For the mechanical behaviour a viscoelastic model coupled with damage concepts is used. The proposed two-step procedure is capable of simulating the behaviour of normal and massive concrete castings under variable ambient conditions, as shown in the examples.

The model has engineering significance from several viewpoints:

(i) It permits the prediction of thermal, hygral and mechanical performance of concrete which is particularly important for bridges, dams, nuclear reactors and other structures with preminent social impact.
(ii) It allows to control the physical and structural response in time with respect to a given mix design and hence to improve the mix design before construction.
(iii) Its flexibility permits to incorporate other features, like durability, attack of pollutant agents to evaluate their effects.[44]

APPENDIX I: CAPILLARY PRESSURE AND WATER POTENTIAL

Equation (4) (i.e. *Kelvin's law*) can be rewritten as

$$P_c = -\rho_l \frac{RT}{M_w} \ln\left(\frac{P_{gw}}{P_{gws}}\right) \tag{15}$$

When a liquid is in equilibrium with its vapour, the specific (mass) Gibbs functions (or thermodynamic potentials) of the two phases are equal and then

$$g_l = g_v \quad \text{and} \quad dg_l = dg_v \tag{16}$$

The differential of the Gibbs function of the vapour dg_v is given by the well-known expression:

$$dg_v = -s_v\,dT + v_v\,dP_{gw} \tag{17}$$

where $v_v = 1/\rho_{gw}$ is the specific (mass) volume of the water vapour and s_v is the specific (mass) entropy of the water vapour. Assuming that the vapour behaves as an ideal gas, i.e. $P_{gw} = \rho_{gw} TR/M_w$ or $P_{gw} = RT/M_w v_v$, (17) becomes

$$dg_v = -s_v\,dT + \frac{RT}{M_w P_{gw}}\,dP_{gw} \tag{18}$$

If we integrate (18), considering an isothermal evolution ($dT = 0$), from the conditions of equilibrium of the vapour with bulk liquid on a flat surface (vapour pressure equal to the vapour tension P_{gws}), up to the actual value of the vapour pressure inside the porous medium, we obtain

$$g_v - g_{v0} = \frac{RT}{M_w} \ln\left(\frac{P_{gw}}{P_{gws}}\right) \tag{19}$$

Equation (19) gives the difference between the Gibbs function of the water inside the porous media in equilibrium with vapour at pressure P_{gw} and the bulk liquid water, at the same temperature. From the thermodynamic point of view, moisture stress or *water potential* Ψ, is then defined as the specific (mass) Gibbs function (or specific thermodynamic potential) of water in a porous medium, referred to pure liquid at the same temperature, and it is given by

$$\Psi = g_v - g_{v0} = \frac{RT}{M_w} \ln\left(\frac{P_{gw}}{P_{gws}}\right) \tag{20}$$

Comparing (20) with (15), it is immediately evident that

$$-\frac{P_c}{\rho_l} = \Psi = \frac{RT}{M_w} \ln\left(\frac{P_{gw}}{P_{gws}}\right) \tag{21}$$

Assuming the liquid incompressible ($\rho_l = cost.$), the capillary pressure P_c is then equal to the water potential Ψ multiplied by a constant ($-\rho_l$). The water potential Ψ is defined for all the conditions of water retained inside a porous medium (monolayer surface adsorption, multilayer surface adsorption and capillary suction) while the capillary pressure P_c has a clear physical meaning, i.e. $P_c = P_g - P_l$, only when liquid water (sometimes called *free* water) is present. Redefining the capillary pressure as $P_c = \rho_l \Psi$, equation (4) or (15) can be used even for water contents below the capillary region.

APPENDIX II: NUMERICAL FORMULATION OF VISCOELASTICITY AND DAMAGE

The numerical formulation here presented is based on the developments presented in Reference 30, where only viscoelasticity was taken into account. The coupling with damage was considered in Reference 21 and will be summarized here, including also anisotropic effects. Indications to include finite strain will be given at the end of this Appendix. The stress–strain relationship used here is a straightforward generalization of the same relation reported in Reference 30. Now

a damage factor $\{\mathbf{1} - \mathbf{D}[\boldsymbol{\varepsilon}^*(t), t]\}$ is also considered:

$$\boldsymbol{\sigma}(t) = [\mathbf{1} - \mathbf{D}(\boldsymbol{\varepsilon}^*(t), t)] \int_0^t \mathbf{C}^{-1} \sum_{\mu=1}^{N} E_\mu(t'_e)\, e^{y_\mu(t'_i) - y_\mu(t_i)} [\mathrm{d}\boldsymbol{\varepsilon}(t') - \mathrm{d}\boldsymbol{\varepsilon}^0(t')] \tag{22}$$

$\mathbf{C}^{-1}$ is eliminated through

$$\mathbf{D}_\mu(t'_e) = \mathbf{C}^{-1} E_\mu(t'_e) \tag{23}$$

yielding

$$\boldsymbol{\sigma}(t) = [\mathbf{1} - \mathbf{D}(\boldsymbol{\varepsilon}^*(t), t)] \int_0^t \sum_{\mu=1}^{N} \mathbf{D}_\mu(t'_e)\, e^{y_\mu(t'_i) - y_\mu(t_i)} [\mathrm{d}\boldsymbol{\varepsilon}(t') - \mathrm{d}\boldsymbol{\varepsilon}^0(t')] \tag{24}$$

Using integration by parts, the previous relation is transformed as follows:

$$\begin{aligned} \boldsymbol{\sigma}(t) = {} & \mathbf{C}^{-1} R(t, t) [1 - \mathbf{D}(\boldsymbol{\varepsilon}^*(t), t)] [\boldsymbol{\varepsilon}(t) - \boldsymbol{\varepsilon}^0(t)] \\ & - [\mathbf{1} - \mathbf{D}(\boldsymbol{\varepsilon}^*(t), t')] \int_0^t \mathbf{C}^{-1}(t'_e) \frac{\partial R(t, t')}{\partial t'} [\boldsymbol{\varepsilon}(t') - \boldsymbol{\varepsilon}^0(t')]\, \mathrm{d}t' \end{aligned} \tag{25}$$

where $\mathbf{C}^{-1} R(t, t)[\mathbf{1} - \mathbf{D}(\boldsymbol{\varepsilon}^*(t), t)]$ represents the stress at time t, due to a unit strain at the same time instant.

Integrating in time by finite differences, when time t is subdivided in n finite intervals $\Delta t = t_{i+1} - t_i$ with $t_1 = 0$ and $t_{n+1} = t$, the following stress–strain relationship is obtained:

$$\begin{aligned} \boldsymbol{\sigma}(t_{n+1}) = {} & [\mathbf{1} - \mathbf{D}(\boldsymbol{\varepsilon}^*(t_{n+1}), t_{n+1})] \sum_{\mu=1}^{N} \mathbf{D}_\mu(t_{e_{n+1}})\, \boldsymbol{\varepsilon}(t_{n+1}) \\ & - [\mathbf{1} - \mathbf{D}(\boldsymbol{\varepsilon}^*(t_{n+1}), t_{n+1})] \sum_{\mu=1}^{N} \mathbf{D}_\mu(t_{e_{n+1}})\, \boldsymbol{\varepsilon}^0(t_{n+1}) \\ & - \frac{1}{2} [\mathbf{1} - \mathbf{D}(\boldsymbol{\varepsilon}^*(t_{n+1}), t_{n+1})] \sum_{\mu=1}^{N} \left\{ \mathbf{D}_\mu(t_{e_{n+1}}) - \mathbf{D}_\mu(t_{e_n})\, e^{(-t_{v_{n+1}} + t_{v_n})/\tau_\eta} \right\} \boldsymbol{\varepsilon}(t_{n+1}) \\ & - \frac{1}{2} [\mathbf{1} - \mathbf{D}(\boldsymbol{\varepsilon}^*(t_{n+1}), t_{n+1})] \sum_{\mu=1}^{N} \left\{ \mathbf{D}_\mu(t_{e_{n+1}}) - \mathbf{D}_\mu(t_{e_n})\, e^{(-t_{v_{n+1}} + t_{v_n})/\tau_\eta} \right\} \boldsymbol{\varepsilon}(t_n) \\ & - \frac{1}{2} [\mathbf{1} - \mathbf{D}(\boldsymbol{\varepsilon}^*(t_{n+1}), t_{n+1})] \sum_{\mu=1}^{N} \mathbf{Q}_{\mu, n+1} \\ & + \frac{1}{2} [\mathbf{1} - \mathbf{D}(\boldsymbol{\varepsilon}^*(t_{n+1}), t_{n+1})] \sum_{\mu=1}^{N} \mathbf{R}_{\mu, n+1} \end{aligned} \tag{26}$$

with $\mathbf{Q}_{\mu, n+1}$ and $\mathbf{R}_{\mu, n+1}$ defined below.

Substituting equation (26) in the equilibrium equation at time t_{n+1} as obtained by the virtual work principle:

$$\int_{(S)} \delta\boldsymbol{\varepsilon}^{\mathrm{T}}\, \boldsymbol{\sigma}(t_{n+1})\, \mathrm{d}V = \delta\mathbf{u}^{\mathrm{T}}\, \mathbf{F}(t_{n+1}) \tag{27}$$

one obtains

$$
\begin{aligned}
&[\mathbf{1} - \mathbf{D}(\boldsymbol{\varepsilon}^*(t_{n+1}), t_{n+1})] \int_{(S)} \delta\boldsymbol{\varepsilon}^{\mathrm{T}} \sum_{\mu=1}^{N} \mathbf{D}_\mu(t_{e_{n+1}})\, \boldsymbol{\varepsilon}(t_{n+1})\, \mathrm{d}V \\
&\quad - \frac{1}{2} \int_{(S)} \delta\boldsymbol{\varepsilon}^{\mathrm{T}} [\mathbf{1} - \mathbf{D}(\boldsymbol{\varepsilon}^*(t_{n+1}), t_{n+1})] \sum_{\mu=1}^{N} \{\mathbf{D}_\mu(t_{e_{n+1}}) - \mathbf{D}_\mu(t_{e_n})\, \mathrm{e}^{(-t_{v_{n+1}} + t_{v_n})/\tau_\eta}\} \boldsymbol{\varepsilon}(t_{n+1})\, \mathrm{d}V \\
&= \int_{(S)} \delta\boldsymbol{\varepsilon}^{\mathrm{T}} [\mathbf{1} - \mathbf{D}(\boldsymbol{\varepsilon}^*(t_{n+1}), t_{n+1})] \sum_{\mu=1}^{N} \mathbf{D}_\mu(t_{e_{n+1}})\, \boldsymbol{\varepsilon}^0(t_{n+1})\, \mathrm{d}V \\
&\quad + \frac{1}{2} \int_{(S)} \delta\boldsymbol{\varepsilon}^{\mathrm{T}} [\mathbf{1} - \mathbf{D}(\boldsymbol{\varepsilon}^*(t_{n+1}), t_{n+1})] \Bigg[\sum_{\mu=1}^{N} \{\mathbf{D}_\mu(t_{e_{n+1}}) \\
&\quad - \mathbf{D}_\mu(t_{e_n})\, \mathrm{e}^{(-t_{v_{n+1}} + t_{v_n})/\tau_\eta}\} \boldsymbol{\varepsilon}(t_n) + \sum_{\mu=1}^{N} \mathbf{Q}_{\mu,n+1} \Bigg] \mathrm{d}V \\
&\quad - \frac{1}{2} \int_{(S)} \delta\boldsymbol{\varepsilon}^{\mathrm{T}} [\mathbf{1} - \mathbf{D}(\boldsymbol{\varepsilon}^*(t_{n+1}), t_{n+1})] \sum_{\mu=1}^{N} \mathbf{R}_{\mu,n+1}\, \mathrm{d}V + \delta\mathbf{u}^{\mathrm{T}} \mathbf{F}(t_{n+1})
\end{aligned} \tag{28}
$$

Introducing spatial approximation by finite elements, the following equilibrium equation can be written:

$$
(\mathbf{K1} - \mathbf{K2})\mathbf{u}(t_{n+1}) = \mathbf{F}(t_{n+1}) + \mathbf{F}_{\mathrm{ML}} + \mathbf{F}_{\mathrm{TH}} + \mathbf{F}_{\mathrm{MTH}} \tag{29}
$$

where

$$
\begin{aligned}
\mathbf{K1} &= \int_{(S)} \mathbf{B}^{\mathrm{T}} [\mathbf{1} - \mathbf{D}(\boldsymbol{\varepsilon}^*(t_{n+1}), t_{n+1})] \sum_{\mu=1}^{N} \mathbf{D}_\mu(t_{e_{n+1}})\, \mathbf{B}\, \mathrm{d}V \\
\mathbf{K2} &= \frac{1}{2} \int_{(S)} \mathbf{B}^{\mathrm{T}} [\mathbf{1} - \mathbf{D}(\boldsymbol{\varepsilon}^*(t_{n+1}), t_{n+1})] \sum_{\mu=1}^{N} \{\mathbf{D}_\mu(t_{e_{n+1}}) - \mathbf{D}_\mu(t_{e_n})\, \mathrm{e}^{(-t_{v_{n+1}} + t_{v_n})/\tau_\eta}\} \mathbf{B}\, \mathrm{d}V \\
\mathbf{F}_{\mathrm{TH}} &= \int_{(S)} \mathbf{B}^{\mathrm{T}} [\mathbf{1} - \mathbf{D}(\boldsymbol{\varepsilon}^*(t_{n+1}), t_{n+1})] \sum_{\mu=1}^{N} \mathbf{D}_\mu(t_{e_{n+1}})\, \boldsymbol{\varepsilon}^0(t_{n+1})\, \mathrm{d}V \\
\mathbf{F}_{\mathrm{ML}} &= + \frac{1}{2} \int_{(S)} \mathbf{B}^{\mathrm{T}} [\mathbf{1} - \mathbf{D}(\boldsymbol{\varepsilon}^*(t_{n+1}), t_{n+1})] \Bigg[\sum_{\mu=1}^{N} (\mathbf{D}_\mu(t_{e_{n+1}}) \\
&\quad - \mathbf{D}_\mu(t_{e_n})\, \mathrm{e}^{(-t_{v_{n+1}} + t_{v_n})/\tau_\eta}\} \boldsymbol{\varepsilon}(t_n) + \sum_{\mu=1}^{N} \mathbf{Q}_{\mu,n+1} \Bigg] \mathrm{d}V \\
\mathbf{F}_{\mathrm{MTH}} &= - \frac{1}{2} \int_{(S)} \mathbf{B}^{\mathrm{T}} [\mathbf{1} - \mathbf{D}(\boldsymbol{\varepsilon}^*(t_{n+1}), t_{n+1})] \sum_{\mu=1}^{N} \mathbf{R}_{\mu,n+1}\, \mathrm{d}V
\end{aligned} \tag{30}
$$

$\mathbf{u}(t_{n+1})$ is the vector of unknown displacements.

In equation (30) $\mathbf{Q}_{\mu,n+1}$ and $\mathbf{R}_{\mu,n+1}$ are respectively defined by

$$
\mathbf{Q}_{\mu,n+1} = \mathrm{e}^{(-t_{v_{n+1}} + t_{v_n})/\tau_\eta} \{[\mathbf{D}_\mu(t_{e_n}) - \mathbf{D}_\mu(t_{e_{n-1}})\, \mathrm{e}^{(-t_{v_n} + t_{v_{n-1}})/\tau_\eta}] [\boldsymbol{\varepsilon}(t_n) - \boldsymbol{\varepsilon}(t_{n+1})] + \mathbf{Q}_{\mu,n}\} \tag{31}
$$

with

$$
\mathbf{Q}_u = \sum_{i=1}^{n-2} \mathrm{e}^{(-t_{v_{n+1}} + t_{v_{i+1}})/\tau_\eta} \{\mathbf{D}_\mu(t_{e_{i+1}}) - \mathbf{D}_\mu(t_{e_i})\, \mathrm{e}^{(-t_{v_{i+1}} + t_{v_i})/\tau_\eta}\} [\boldsymbol{\varepsilon}(t_{i+1}) - \boldsymbol{\varepsilon}(t_i)] \tag{32}
$$

$$
\mathbf{R}_{\mu,n+1} = [\mathbf{D}_\mu(t_{e_{n+1}}) - \mathbf{D}_\mu(t_{e_n})\, \mathrm{e}^{(-t_{v_{n+1}} + t_{v_n})/\tau_\eta}] [\boldsymbol{\varepsilon}^0(t_n + 1) - \boldsymbol{\varepsilon}^0(t_n)] + \mathrm{e}^{(-t_{v_{n+1}} + t_{v_n})/\tau_\eta} \mathbf{R}_{\mu,n} \tag{33}
$$

with

$$\mathbf{R}_{\mu 1} = \sum_{i=1}^{n-1} \mathrm{e}^{(-t_{v_n} + t_{v_{i+1}})/\tau_\eta} \{\mathbf{D}_\mu(t_{e_{i+1}}) - \mathbf{D}_\mu(t_{e_i})\mathrm{e}^{(-t_{v_{i+1}} + t_{v_i})/\tau_\eta}\} [\boldsymbol{\varepsilon}(t_{i+1}) - \boldsymbol{\varepsilon}(t_i)] \tag{34}$$

Equation (26) can be rewritten in compact form as follows:

$$\boldsymbol{\sigma}(t_{n+1}) = [\mathbf{1} - \mathbf{D}(\boldsymbol{\varepsilon}^*(t_{n+1}), t_{n+1})][C_1 \boldsymbol{\varepsilon}(t_{n+1}) + C_2 \boldsymbol{\varepsilon}^0(t_{n+1}) + C_3 \boldsymbol{\varepsilon}^0(t_n) - \frac{1}{2}\sum_{\mu=1}^{N} \mathbf{Q}_{\mu,n+1} + \frac{1}{2}\sum_{\mu=1}^{N} \mathbf{R}_{\mu,n+1}] \tag{35}$$

where

$$\begin{aligned} C_1 &= \sum_{\mu=1}^{N} [\mathbf{D}_\mu(t_{e_{n+1}}) - \tfrac{1}{2}[\mathbf{D}_\mu(t_{e_{n+1}}) - \mathbf{D}_\mu(t_{e_n})\mathrm{e}^{(-t_{v_{n+1}} + t_{v_n})/\tau_\eta}]] \\ C_2 &= -\sum_{\mu=1}^{N} \mathbf{D}_\mu(t_{e_{n+1}}) \\ \mathbf{C}_3 &= -\frac{1}{2}\sum_{\mu=1}^{N} [\mathbf{D}_\mu(t_{e_{n+1}}) - \mathbf{D}_\mu(t_{e_n})\mathrm{e}^{(-t_{v_{n+1}} + t_{v_n})/\tau_\eta}] \end{aligned} \tag{36}$$

The relations are used in the non-linear formulation reported in the paper, where stress and strain measures were replaced by the corresponding ones in finite strains.

APPENDIX III: NON-LOCAL DAMAGE MODEL

A non-local formulation is also used in this paper to better model the damage effects of concrete and to obtain objective solutions, with respect to the adopted discretizations.[45]

The non-local model adopted is based on the following assumption to evaluate the strain variable ε:

$$\varepsilon(\mathbf{x}) = \frac{1}{V_r(\mathbf{x})}\int_V \varepsilon^*(\mathbf{s})\alpha(\mathbf{s} - \mathbf{x})\,\mathrm{d}V \tag{37}$$

where ε is the equivalent strain (in Mazars' model), $\mathbf{x}$ is the coordinate of the current Gauss point $\mathbf{s}$ the coordinate of the generic Gauss point, α the weight function defined as $\alpha(\mathbf{s} - \mathbf{x}) = \mathrm{e}^{(k\|\mathbf{s}-\mathbf{x}\|/l)^2}$ and V_1 the characteristic volume defined as $V_r(\mathbf{x}) = \int_V \alpha(\mathbf{s} - \mathbf{x})\,\mathrm{d}V$. Constant k in two-dimensional problems is equal to 2; l is the so called characteristic length. Typically $l \cong 2{\cdot}8\,\mathrm{d_a}$, where $\mathrm{d_a}$ is the maximum dimension of concrete aggregate. The meaning of V_r is similar to that of a representative elementary volume in heterogeneous materials theory.

In this model the only non-local variable is the strain controlling damage, e.g. the strain related to the strain-softening branch of the stress–strain diagram of concrete. All the other other variables are computed in a local manner.

NOTATION

$\mathbf{B}_0$ initial strain matrix
$\mathbf{B}_L$ linear strain matrix
C_p effective specific heat of the porous material, $\mathrm{J\,kg^{-1}\,K^{-1}}$
C_{pg} specific heat of the gas mixture, $\mathrm{J\,kg^{-1}\,K^{-1}}$
C_{ps} specific heat of the solid matrix, $\mathrm{J\,kg^{-1}\,K^{-1}}$

C_{pl} specific heat of the liquid phase (water), $J\,kg^{-1}\,K^{-1}$
$\mathbf{C}_i$ viscoelastic dependent terms ($i = 1, \ldots, 3$)
D_{eff} effective diffusivity of the gas mixture, $m^2\,s^{-1}$
$\mathbf{D}$ damage tensor
$\mathbf{E}$ Green–Lagrange strain tensor
$\mathbf{E}^0$ autogeneous Green–Lagrange strain tensor
$\mathbf{g}$ gravity acceleration vector ($= 9{\cdot}80665\,m\,s^{-2}$)
$\mathbf{G}$ non-linear strain matrix
$\mathbf{J}$ Jacobian matrix
K absolute permeability, m^2
K_{rg} relative permeability of the gas phase
K_{rl} relative permeability of the liquid phase
M molar mass of the gas moisture (moist air), $kg\,kmol^{-1}$
M_a molar mass of the dry air, $kg\,kmol^{-1}$
M_w molar mass of the water vapour, $kg\,kmol^{-1}$
P_c capillary pressure, Pa
P_g pressure of the gas phase, Pa
P_{gw} water vapour partial pressure, Pa
P_{gws} water vapour saturation pressure, Pa
$\mathbf{Q}_\mu$ load vector of the Maxwell chain units
R gas constant ($8314{\cdot}41\,J\,kmol^{-1}\,K^{-1}$)
$\mathbf{R}$ external virtual work vector, N
$\mathbf{R}_\mu$ load vector of the Maxwell chain units
S liquid-phase volume saturation (liquid vol./pore vol.)
$\mathbf{S}$ second Piola–Kirchhoff stress tensor, Pa
t time variable, s
T temperature, K
$\mathbf{u}$ displacement vector, m
V volume reference, m^3
$\mathbf{x}$ point coordinates, m

Greek symbols

Δh_{vap} enthalpy of vaporization per unit mass, $J\,kg^{-1}$
$\boldsymbol{\varepsilon}$ infinitesimal strain tensor
$\boldsymbol{\varepsilon}^0$ infinitesimal autogeneous strain tensor
$\boldsymbol{\eta}$ non-linear component of the strain tensor
λ_{eff} effective thermal conductivity, $W\,m^{-1}\,K^{-1}$
μ_g gas-phase dynamic viscosity, $Pa\,s^{-1}$
μ_l liquid-phase dynamic viscosity, $Pa\,s^{-1}$
ρ effective density of the porous medium, $kg\,m^{-3}$
ρ_g gas-phase density, $kg\,m^{-3}$
ρ_{ga} mass concentration of dry air in the gas phase, $kg\,m^{-3}$
ρ_{gw} mass concentration of water vapour in the gas phase, $kg\,m^{-3}$
ρ_l liquid-phase density, $kg\,m^{-3}$
σ surface tension, $N\,m^{-1}$
$\boldsymbol{\sigma}$ Cauchy stress tensor, Pa
ϕ porosity (=pore vol./total vol.)

REFERENCES

1. H. Glaser, 'Warmeleitung und Feuchtigkeitsdurchgang durch Kuhlraumisolierungen' *Kaltechnik*, **10**(3), 86–91 (1958).
2. H. Glaser, 'Temperatur- und Dampfdruckverlauf in einer homogenen Wand bei Feuchtigkeitsausscheidung' *Kaltechnik* **10**(6), 174–179 (1958).
3. H. Glaser, 'Graphisches Verfahren zur Untersuchung von Diffusionvorgangen' *Kaltechnik*, **11**(10), 345–349 (1959).
4. J. R. Philip, D. A. De Vries, 'Moisture movements in porous material under temperature gradients', *Trans. Am. Geophys. Union*, **38**(2), 222–232 (1957).
5. D. A. De Vries, 'Simultaneous transfer of heat and moisture in porous media', *Trans. Am. Geophys. Union*, **39**(5), 909–916 (1958).
6. S. Whitaker, 'Simultaneous heat mass and momentum transfer in porous media: a theory of drying', in: *Advances in heat transfer. Vol.* 13, Academic Press, New York, 1977.
7. A. V. Luikov, *Heat and Mass Transfer in Capillary Porous Bodies*, Pergamon, London 1966.
8. P. Chen, D. C. T. Pei, 'A mathematical model of drying processes', *Int. J. Heat Mass Transfer*, **32**(2), 297–310 (1989).
9. S. Whitaker, 'Heat and mass transfer in granular porous media, in *Adv. Drying*, *Vol.* 1, Hemisphere, New York, 1980.
10. J. Bear, *Dynamics of Fluids in Porous Media*, Dover, New York, 1988.
11. J. Bear, *Hydraulics of Groundwater*, Mc Graw Hill, New York, 1979.
12. J. Bear, Y. Bachmat, *Introduction to Modelling of Transport Phenomena in Porous Media*, Kluwer, Dordrecht, 1990.
13. Y. Bachmat, J. Bear, 'Macroscopic modelling of transport phenomena in porous media. 1: the continuum approach', *Transp. Porous Media*, **1**, 213–240 (1986).
14. J. Bear, Y. Bachmat, 'Macroscopic modelling of transport phenomena in porous media. 2: applications to mass momentum and energy transfer', *Transp. Porous Media*, **1**, 241–269 (1986).
15. M. Hassanizadeh, W. G. Gray, 'General conservation equations for multiphase systems: 1 Averaging technique', *Adv. Water Res.*, **2**, 131–144 (1979).
16. M. Hassanizadeh, W. G. Gray, 'General conservation equations for multiphase systems: 2 Mass, momenta, energy and entropy equations', *Adv. Water Res.*, **2**, 191–203 (1979).
17. M. Hassanizadeh, W. G. Gray, 'General conservation equations for multiphase systems: 3 Constitutive Theory for Porous Media Flow', *Adv. Water Res.*, **3**, 25–40 (1980).
18. S. B. Nasrallah, P. Perre, 'Detailed study of a model of heat and mass transfer during convective drying of porous media', *Int. J. Heat Mass Transfer*, **31**(5), 957–967 (1988).
19. M. Ilic, I. W. Turner, 'Convective drying of a consolidated slab of wet porous material', *Int. J. Heat Mass Transfer*, **32**(12), 957–967 (1989).
20. M. Ilic, I. W. Turner, 'Convective drying of a consolidated slab of wet porous material including the sorption region', *Int. Commun. Heat Mass Transfer*, **17**, 39–48 (1990).
21. C. E. Majorana, 'Influence of damage in thermohygrometric and mechanical behaviour of the continuum', *Giornale del Genio Civile*, **7–9**, 211–236 (in Italian) (1989).
22. J. Lemaitre, J. L. Chaboche, *Mechanique des materiaux solides*, Dunod, Paris, 1988.
23. Z. P. Bazant, S. Prasannan, 'Solidification theory for concrete creep. II—verification and application', *J. Eng. Mech.*, **115**(8), 1704–1725 (1989).
24. S. Ramtani, 'Contribution a la modelisation du comportment multiaxial du béton endommagé avec description du caractére unilatéral', *Thèse de doctorat présentée a l'Université Pierre et Marie Curie*, Paris, 1990.
25. L. M. Kachanov, 'Introduction to continuum damage mechanics', in H. H. E. Leipholz and G. Gravas (eds.), *Mechanics of Elastic Stability*, Martinus Nijhoff, Dordrecht, 1986.
26. R. W. Lewis, C. E. Majorana, B. A. Schrefler, 'A coupled finite element model for the consolidation of nonisothermal elastoplastic porous media', *Transp. Porous Media.* **1**, 155–178 (1986).
27. R. W. Lewis, P. J. Roberts, B. A. Schrefler, 'Finite element modelling of two-phase heat and fluid flow in deforming porous media', *Transp. Porous Media*, **4**, 319–334 (1989).
28. R. B. Bird, E. W. Stewart, E. N. Lightfoot, *Transp. Phenomena*, Wiley, New York, 1960.
29. P. Baggio, C. Bonacina, *Introduction to Modelling Heat and Mass transfer in Porous Building Materials*, Quaderno di Istituto n. 146, - Istituto di Fisica Tecnica dell' Università di Padova, in press.
30. C. E. Majorana, R. Vitaliani, 'Numerical modelling of creep and shrinkage of concrete by finite element method', *Proc. 2nd Int. Conf. on Computer Aided Design in Concrete Structures.* SCI-C, Zell-Am-Sec, Austria, 4–6 April 1990, pp. 773–784.
31. B. A. Schrefler, 'Recent advances in numerical modelling of geomaterials', *Meccanica* **26**(2/3), 93–101 (1991).
32. J. Mazars, G. Pijaudier-Cabot, 'Continuum damage theory—application to concrete', *J. Eng. Mech.*, ASCE, **115**(2), 345–365 (1989).
33. J. E. Marsden, T. J. R. Hughes, *Mathematical Foundations of Elasticity*, Prentice Hall, Englewood Cliffs, N.J., 1982.
34. K. J. Bathe, *Finite Element Procedure in Engineering Analysis*, Prentice-Hall, Englewood Cliffs, NJ, 1982.
35. C. E. Majorana, R. Vitaliani, 'Analisi termomeccanica non-lineare per geometria e materiali dei corpi continui discretizzati con elementi finiti', *Giornale del Genio Civile*, (1–3), 39–82 (1990).
36. J. C. Simo, 'On a fully three-dimensional finite-strain viscoelastic damage model: formulation and computational aspects', *Comput. Methods Appl. Mech. Eng.*, 153–173 (1987).
37. O. C. Zienkiewicz, R. L. Taylor, *The Finite Element Method*, 4th Edn, Mc Graw Hill, London 1989 (Vol. 1) and 1991 (Vol. 2).

38. B. Schrefler, L. Simoni, C. Majorana, 'A general model for the mechanics of saturated unsaturated porous materials', *Mater. Struct.*, **22,** 323–334 (1989).
39. P. Acker, G. Abiar, Y. Malier, 'Modèle de comportement différée du béton prenant en compte de l'hygrometrie locale', Laboratorie Centrale des Ponts et Chaussées, Paris, France, 1986.
40. S. Nagamatsu, Y. Sato, 'Experimental studies of creep rupture and defomation of cement mortar under high structural compressive load', *Rew. of 31th gen. meet.*, The Cement Ass. of Japan, pp. 196–198 (1977) (in Japanese).
41. M. Mamillan, A. Boineau, 'Measure de l'humidité dans le matériaux en place', *Annales de l'ITBTP*, **382,** 158–167 (1980).
42. Z. P. Bazant, L. J. Najjar, 'Non-linear water diffusion in nonsaturated concrete', *Mater. Struct.*, **5**(25), 3–20 (1972).
43. F. H. Wittmann, P. E. Roelfstra, 'Numerical analysis of drying and shrinkage', in *Autoclaved Aerated Concrete, Moisture Content and Properties*, Elsevier, Amsterdam, 1989.
44. A. V. Saetta, B. A. Schrefler, R. Vitaliani, 'The carbonation of concrete and the mechanism of moisture, heat and carbon dioxide flow through porous materials, *Int. J. Cement and Concrete Research*, **23,** 761–772 (1993).
45. G. Pijaudier-Cabot, 'Finite element analysis of bifurcation in nonlocal strain softening solids', *Proc. 2nd World Congress on Computational Mechanics*, Stuttgart, 1990.